Applied Soft Computing xxx (2016) xxx–xxx

Contents lists available at ScienceDirect

Applied Soft Computing

journal homepage: www.elsevier.com/locate/asoc

Distribution network fault section identification and fault location using wavelet entropy and neural networks

Adeyemi Charles Adewole*, Raynitchka Tzoneva, Shaheen Behardien

Centre for Substation Automation and Energy Management Systems (CSAEMS), Cape Peninsula University of Technology, Cape Town, South Africa

ARTICLE INFO

Article history:
Received 30 January 2014
Received in revised form 25 February 2016
Accepted 8 May 2016
Available online xxx

Keywords:
Artificial neural network
Discrete waveform transform
Fault location
Fault section identification
Wavelet energy spectrum entropy

ABSTRACT

Fault location in power system distribution networks is especially difficult because of the existence of several laterals/tap-offs in distribution networks. This implies that the calculated fault point can be wrongly estimated to be in any of the laterals. This paper proposes a new hybrid method combining Discrete Wavelet Transform (DWT) and artificial neural network (ANN) for fault section identification (FSI) and fault location (FL) in power system distribution networks. DWT was used in the analysis and extraction of the characteristic features from fault transient signals of the three phase line current measurements obtained at a single substation relaying point, rather than the double-ended approach used in the existing literature. Entropy Per Unit (EPU) indices are afterwards computed from the DWT decomposition, and are used as input to multi-layer ANN models serving as FSI classifiers and FL predictors respectively. The proposed hybrid method is tested using a benchmark IEEE 34-node test feeder. Comparisons, verification, and analysis made using the experimental results obtained from the application of the method showed very good performance for different fault types, fault locations, fault inception angles, and fault resistances. The proposed hybrid method is unique because of the pre-processing stage done with the DWT-EPU indices, the use of only line current measurements from a single relaying point, and the division of the FSI and FL tasks into sub-problems with respective ANN models.

1. Introduction

Electric power interruptions are characterized by standard reliability indices. These indices measure the system performance and reflect the status of the overall performance/Quality of Service (QoS) of a particular network at the load points. The most commonly used indices in utility companies are the System Average Interruption Frequency Index (SAIFI) and the System Average Interruption Duration Index (SAIDI). SAIFI is the mean of the number of interruptions a customer experiences, and it is measured in units of interruptions/customer over a year. SAIDI is the system average interruption duration per customer per year. This index is commonly referred to as customer minutes of interruption. In order to maintain a good QoS and facilitate the timely restoration of power, there is the need for effective fault diagnosis methods to improve the reliability of distribution networks when faults occur. The identification and location of faults is difficult in distribution networks because of the non-homogeneity of lines along a typical distribution feeder. Also, the presence of laterals (branches), distributed loads, and frequent modifications in the feeder configuration, makes distribution networks distinct. The early detection and diagnosis of faults would expedite service restoration and help reduce downtime.

Fault section identification (FSI) is the identification of the faulted section in the distribution system, while fault location (FL) is the estimation of the distance to the fault point from the substation relaying point. When faults occur in distribution lines, the transient features are distinct and the high frequency components in the transients can be employed to reveal fault characteristics. Diagnostic methods are broadly classified into impedance/other fundamental frequency methodologies, high frequency components/travelling wave methodologies, and knowledge based methodologies [1,2]. Fault location in transmission networks is widely reported in the literature. Impedance-based methods for transmission networks have been proposed in Refs. [3–6], while Refs. [7,8] made use of artificial neural networks (ANNs). Similarly, Bhowmik et al. [9] used a method based on wavelet analysis and ANN. Hongchun and Xiangfei [10] proposed a method based on rough sets and ANN, while Sadeh and Afradi [11] used an adaptive network-based fuzzy inference system. However, methods designed for transmission networks are prone to errors

* Corresponding author.
E-mail addresses: adewolea@cput.ac.za, yemmyadewole@yahoo.co.uk (A.C. Adewole).

http://dx.doi.org/10.1016/j.asoc.2016.05.013
1568-4946/

because of the dissimilarity between transmission and distribution networks. This is because distribution lines are non-homogeneous with different conductor sizes. Also, the presence of laterals/tap-offs, radial operation, inaccuracies in the configuration of the feeder, unbalanced phases, varying fault resistance, and load taps along distribution lines make distribution networks distinct. Therefore, fault diagnosis in distribution networks is beginning to attract the attention of researchers.

Methods based on impedance calculations [12–19], wavelet and travelling wave theory [20–28], computational intelligence [29–34], and hybrid methods [35,36], have been proposed for distribution networks fault location. Most of the existing methods make use of current and voltage quantities which add to the computational effort and processing time. This also implies that Voltage Transformers (VTs) and Current Transformers (CTs) would be required for real world implementation in substations. However, the substations in distribution networks only have CTs (current measurement), usually for overcurrent protection relays (ANSI 50/51). Furthermore, the impedance and fundamental frequency based method suffer from limitations due to the loading of the line, fault path resistance, admittance matrix manipulation, harmonic components in the current source parameters, measurement error, and load imbalance. There is also the possibility of multiple estimation due to the existence of multiple possible fault locations in the distribution network. The shortcomings of the travelling wave methodology include the high implementation costs, complexity, the need for high sampling rate, sophisticated measuring equipment, and the need for synchronization/communication for double-ended methods. This is further exacerbated by the discontinuities caused by the numerous sub-feeders that are characteristic of radial distribution systems. The discontinuities may be between the end of the line and the fault point, and these add up the reflections to the transient waves from the fault. The techniques in the knowledge-based method are regarded as complex and the computational costs may be high in applications involving a high number of faults.

From the foregoing, it can be seen that many diagnostic methods have been developed and proposed, but a perfect, dependable, and secure method is still needed. In this paper, a new 2-stage method based on the hybrid integration of wavelet transform and artificial neural network is proposed for fault section identification and fault location in power system distribution networks. The proposed fault section identification stage is initiated before the fault location stage in order to solve the distribution network multiple estimation problem whereby multiple laterals corresponds to the calculated fault point. The contribution of this paper can be summarized as follows: (i) the development of a non-iterative 2-stage predictive hybrid method comprising of the identification of the faulted section and the fault location in distribution systems, (ii) the application of a frequency-time wavelet energy entropy technique designed to capture the transient information that are present in the signal during faults, (iii) the use of single-ended measurements only, and (iv) the development of an accurate hybrid method for FSI and FL using line current measurements only.

This paper is divided into the following sections: Section 2 describes the proposed method based on wavelet transform and neural network. The implementation of the fault section identification and fault location algorithms are outlined in Section 3. Section 4 discusses the results of this approach, while Section 5 summarizes the conclusion.

2. The proposed wavelet transform-neural network method

The aim of the proposed method is the identification of the faulted section and the location of the point where the fault is, in a given power system distribution network. This is carried out after the fault has been detected in the distribution network and the type of fault has been classified as proposed by the authors in Refs. [37,38]. The proposed hybrid method is developed to satisfy the following criteria: (i) take into account the specific nature of power system distribution networks and the scenarios that are likely to occur, (ii) to use line current measurements obtained from the three phases and zero sequence currents measured in the distribution network as the input data to the proposed method, (iii) the extraction of significant information that can represent the fundamental characteristics of the measured signal from a disturbance waveform, and (iv) the ability of the proposed method to take fast decision on the basis of the extracted disturbance waveform.

The steps involved in the implementation of the proposed hybrid method are detailed below: (i) the specific feature extraction of the fault signal obtained through the application of the Discrete Wavelet Transform (DWT) and the computation of the Wavelet Energy Entropy (WEE), and (ii) fast decision making for the identification of the faulted section and the location of the fault point through the training of artificial neural network models using the extracted DWT WEE and the computed Entropy Per Unit (EPU) as inputs.

Fig. 1 illustrates the above-mentioned steps, and the theoretical background of the methods involved are given in the proceeding sections.

2.1. Wavelet transform

Although, the Fourier transform (FT) has been used in several fields for signal processing, its application for transient signals is limited by the fact that fault transients are non-stationary and there is the need to analyze them at various transitions as the signal changes. Short-Time Fourier Transform (STFT) was introduced to correct the shortcoming of the FT. However, a fixed time window is used.

A technique such as wavelet transform (WT) capable of multiple resolutions in time and frequency, with a flexible window size suitable for non-stationary signals is thereby required.

The windowing in WT automatically uses short time intervals for high frequency components, and long time intervals for low frequency components determined by using the scaling and shifting techniques. Discrete Wavelet Transform (DWT) is a variant of WT, and it is a versatile signal processing technique widely applied in many engineering and scientific fields. One area in which the DWT has been particularly successful is for transient analysis in power systems [39–42]. This is because it acquires the transient features and accurately analyzes them in both the time and frequency contexts at different frequency bands, and with different resolutions by decomposing the signal into a coarse approximation and detail components. It employs two sets of functions, called the scaling function ϕ and the wavelet function ψ, which are related to low pass and high pass filters, respectively.

The mathematical expression for DWT is given by Refs. [40,41,43,44]:

$$\mathrm{DWT}(m,n) = \frac{1}{\sqrt{2^m}} \sum_k f(k)\psi\left(\frac{n-k2^m}{2^m}\right) \quad (1)$$

where $f(k)$ is the discrete signal represented as a function of its coefficients, $\psi(.)$ is the mother wavelet (window function), m and n are the time scale parameters, k is both the discrete time and the number of coefficients in the DWT, 2^m is the variable for scaling, $k2^m$ is the variable for shifting, and $1/\sqrt{2^m}$ is the energy normalization component to ensure the same scale as the mother wavelet.

The original signal sequence $f(k)$ can also be represented by a sum of all components. That is, the sum of all the details and the

Please cite this article in press as: A.C. Adewole, et al., Distribution network fault section identification and fault location using wavelet entropy and neural networks, Appl. Soft Comput. J. (2016), http://dx.doi.org/10.1016/j.asoc.2016.05.013

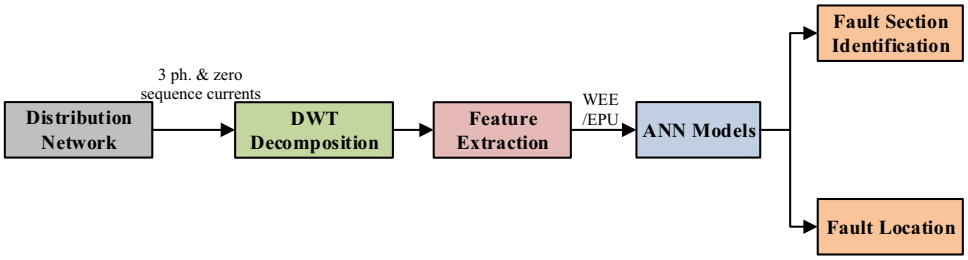

Fig. 1. A summary of the proposed fault section identification and fault location algorithms in the proposed method.

approximation components at the last level of decomposition. For example, for two levels of decomposition, the representation is:

$$f(k) = c_1 D_1(k) + c_1 A_1(k) = c_1 D_1(k) + c_2 D_2(k) + c_2 A_2(k) \quad (2)$$

where D_1 and D_2 are the detail components of the first and second decomposition levels respectively, A_1 and A_2 are the approximation components of the first and second decomposition levels, c_j is the coefficient of the detail or approximation components at the jth decomposition level, and $c_1 A_1(k) = c_2 D_2(k) + c_2 A_2(k)$.

In the implementation of Multi Resolution Analysis (MRA) for DWT, the scaling and wavelet functions are given by [20]:

$$\phi_{m,n}(t) = 2^{-(m/2)} \phi \left(2^{-m} t - n\right) \quad (3)$$

$$\psi_{m,n}(t) = 2^{-(m/2)} \psi \left(2^{-m} t - n\right) \quad (4)$$

where $\phi_{m,n}(t)$ is the scale function, and $\psi_{m,n}(t)$ is the wavelet function of time t.

Wavelets are localized in both time (through translation operation) and frequency (through dilation operation). The first scale covers a broad frequency range at the high frequency end of the spectrum and the higher scales cover the lower end of the frequency spectrum. The decomposition of the signal starts by passing it through a set of filters. The approximations are the high-scale, low-frequency components of the signal produced by filtering with a low-pass filter (h). The details are the low-scale, high-frequency components of the signal produced by a high-pass filter (g). The bandwidth of these two filters is equal but (h) is the reversed version of (g). After the first decomposition of the signal, the sampling frequency is decreased by half. To obtain the components of the next DWT level, the low-pass filter output (approximation) is decomposed. Daubechies-4 (db4) is one of the most used wavelet in power system disturbance analysis and it was chosen to analyze the fault signals in this paper because of its orthogonality, compact support in the time domain, and for its good performance in power system studies as reported by Refs. [39,40].

2.2. Wavelet energy spectrum entropy

Fault signals are known to contain transients and harmonics. The direct use of these signals would result to classifiers and predictors with poor performance. Thus, feature extraction should be carried out in order to identify attributes (features) which best represent the characteristics of the fault signal. Wavelet Energy Entropy (WEE), which evolved from Shannon entropy [39–41] is capable of giving the energy information in signals or systems. Since fault signals have high frequency components, it is more distinctive to use the energy of the detail coefficients to extract the characteristics of the fault signals.

The wavelet energy of a signal at a scale j and an instant k is given as [39–41]:

$$E_{jk} = |D_j(k)|^2 \quad (5)$$

At the jth scale, the instants are $k = 1, 2, 3, \ldots, N$, where N is the number of instants (coefficients) in the jth scale, L is the number of decomposition levels. The summation of the signal wavelet energy spectrum at the jth scale is:

$$E_j = \sum_{k=1}^{N} E_{jk}, \quad j = \overline{1, L} \quad (6)$$

The relative wavelet energy is given as [40]:

$$P_{jk} = \frac{E_{jk}}{E_j}, \quad j = \overline{1, L} \quad (7)$$

The wavelet energy ratio (Eq. (7)) represents the energy distribution. Therefore, the wavelet energy entropy (WEE) is given by [40,41]:

$$\mathrm{W}_{\mathrm{EE}jp} = -\sum_{k} P_{jkp} \log P_{jkp}, \quad j = \overline{1, L} \quad (8)$$

where $p \in \{A, B, C\}$ are phases of the distribution network.

The wavelet Entropy Per Unit index is proposed as:

$$\mathrm{EPU}_{jp} = \frac{-\sum_{k} P_{jkp} \log P_{jkp}}{\left(-\sum_{k} P_{jkA} \log P_{jkA}\right) + \left(-\sum_{k} P_{jkB} \log P_{jkB}\right) + \left(-\sum_{k} P_{jkC} \log P_{jkC}\right)} \quad (9)$$

Eq. (9) forms the basis for the feature extraction and selection process. The extracted features are used as inputs to the ANN models trained to identify the faulted section and the location of the fault point respectively.

2.3. Fault section identification ANN design

Four categories of faults are possible in a distribution network. These are (i) single line-to-ground (1 Ph.g) faults, (ii) two phase (2 Ph.) faults, (iii) two phase-to-ground (2 Ph.g) faults, and (iv) three phase (3 Ph.) faults. In view of the above, individual ANN model are trained for the identification of the faulted section depending on the type of fault detected in the system. Using an ANN model for each fault type increases the learnability of the ANN model, reduces the size of the hidden layer neuron, and improves the accuracy of the ANN model. Thus, the proposed FSI algorithm consists of four back-propagation ANN models. During the training of the ANNs, each ANN acquires knowledge about the problem from the training dataset, and stores the knowledge acquired using synaptic weights between the neurons.

Exploratory experimentation involving various numbers of hidden layers, hidden layer neurons, learning rate, and activation functions was carried out. Sigmoid activation functions (*tansig*) are

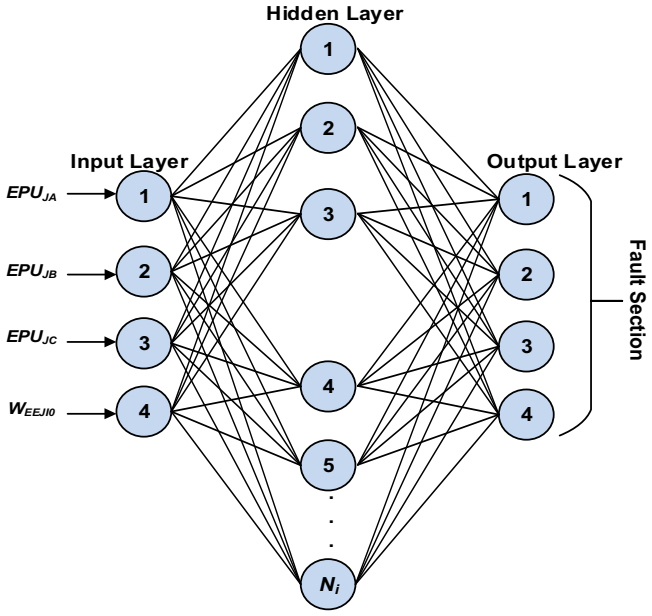

Fig. 2. Architecture of the ANN model for the fault section identification task.

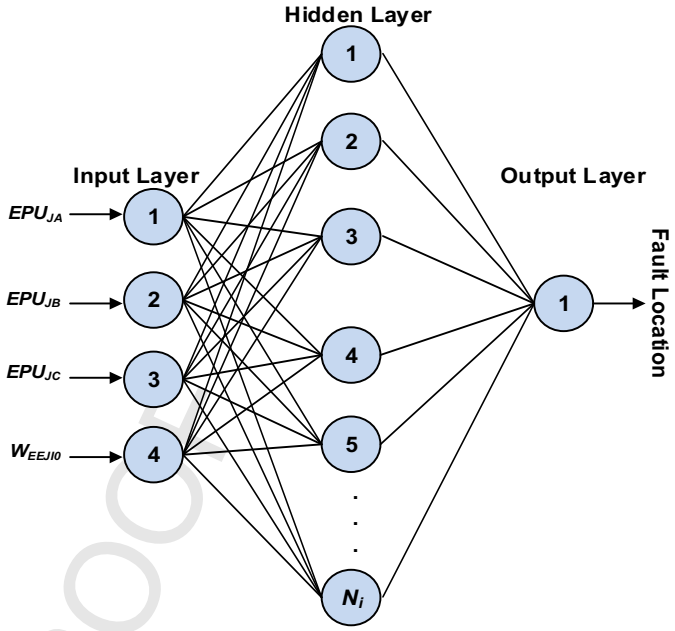

Fig. 3. Architecture of the ANN model for the fault location task.

used for the hidden and output layers of the FSI ANN models. The *logsimoid* and *purelin* activation functions were also experimented upon, but were found to give poor performances. Fig. 2 shows the structure of the ANN model designed for the FSI task.

2.4. Fault location ANN design

Similar approach to the FSI task was followed in the design of the fault location (FL) algorithm. The FL is decomposed into four regression tasks corresponding to the four classes of faults that can occur in distribution networks. Thus, ANN models for fault location are developed for 1 Ph.g, 2 Ph., 2 Ph.g, and 3 Ph. faults respectively. The designed ANN models take in sets of four inputs of EPU/WEE of the three phase and zero sequence line currents, and one output node that gives the estimated distance of the fault in kilometres (km). The sigmoid activation function (*tansig*) was used in the hidden layer, while the linear activation function (*purelin*) was used in the output layer.

The performance criteria used in the selection of the optimal ANN model are the neural network size (number of hidden layer neurons), correlation coefficient, error histogram, and testing with untrained datasets. The accuracy of the untrained datasets is determined by the percentage error of the ANN accuracy. Fig. 3 shows the structure of the ANN model designed for the FL task.

2.5. Proposed algorithm

The algorithms for the implementation of the proposed 2-stage hybrid method are shown in Fig. 4. The fault signal waveforms are decomposed using DWT. EPU is afterwards computed and used as the input to the ANN model. The particular ANN model to use is determined through the use of the fault-type classification algorithm proposed by the authors in Refs. [37,38]. The algorithms for the proposed hybrid method are implemented as described in Section 3 of this paper.

3. Implementation of the proposed method

3.1. Modelling: IEEE 34- Node Benchmark Test Feeder

The testing and validation of the proposed hybrid method was carried out using the IEEE 34 Node Test feeder [45]. The IEEE 34 Node Test Feeder is a long feeder with unbalanced loading and nominal voltage of 24.9 kV. The total feeder load equals 2060 kW and the 2500 kVAr. Fig. 5 shows the IEEE 34 Node Test Feeder. Modelling of this distribution network was done in DIgSILENT PowerFactory. Binary notations have been inserted on the test feeder to denote the various fault sections as shown in Fig. 5.

3.2. Simulations using the test feeder

ElectroMagnetic Transient (EMT) simulations consisting of different fault types at different locations with various fault resistances (R_f) and fault inception angles (θ_{fA}) were performed. A waveform window of 10 cycles obtained from the EMT simulations was used. Voltage sags and current swells are usually experienced at the faulted phase(s) during fault conditions. The magnitude of these sags or overcurrents depends on the type of the fault and the system parameters. Three phase line currents and zero sequence current of the various simulation waveforms were exported to MATLAB for signal processing. Tables 1 and 2 give the parameters

Table 1
ANN training simulation parameters.

Parameter	Main feeder (%)	Lateral section (%)
Fault location (%)	10, 20, 30, 40, 50, 60, 70, 80, 90, 95	5, 25, 50, 75, 95
Fault resistance (Ω)	0, 20, 100	0, 20, 100
Fault inception angle (°)	0, 30, 60, 90	0, 30, 60, 90
Fault type	Single phase-to-ground (1 Ph.-g), Two phase (2 Ph.), Two phase-to-ground (2 Ph.-g), and Three phase (3 Ph.)	Single phase-to-ground (1 Ph.-g), Two phase (2 Ph.), Two phase-to-ground (2 Ph.-g), and Three phase (3 Ph.)

Please cite this article in press as: A.C. Adewole, et al., Distribution network fault section identification and fault location using wavelet entropy and neural networks, Appl. Soft Comput. J. (2016), http://dx.doi.org/10.1016/j.asoc.2016.05.013

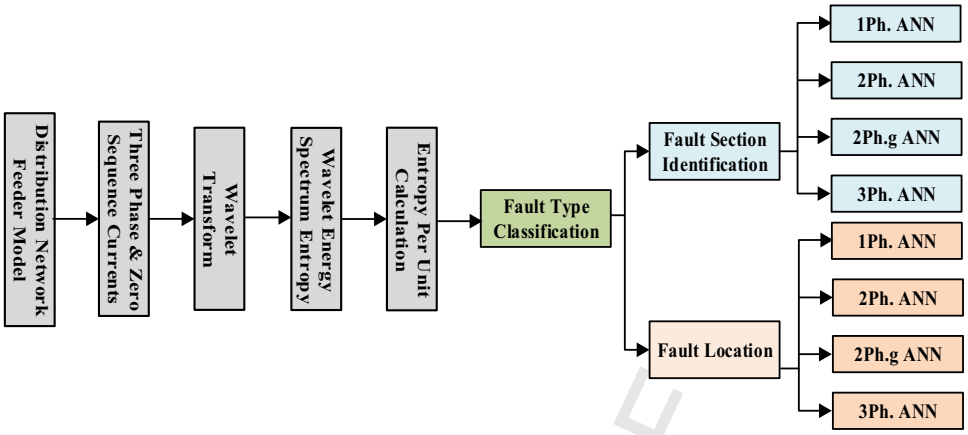

Fig. 4. Functional block diagram of the proposed hybrid diagnostic method.

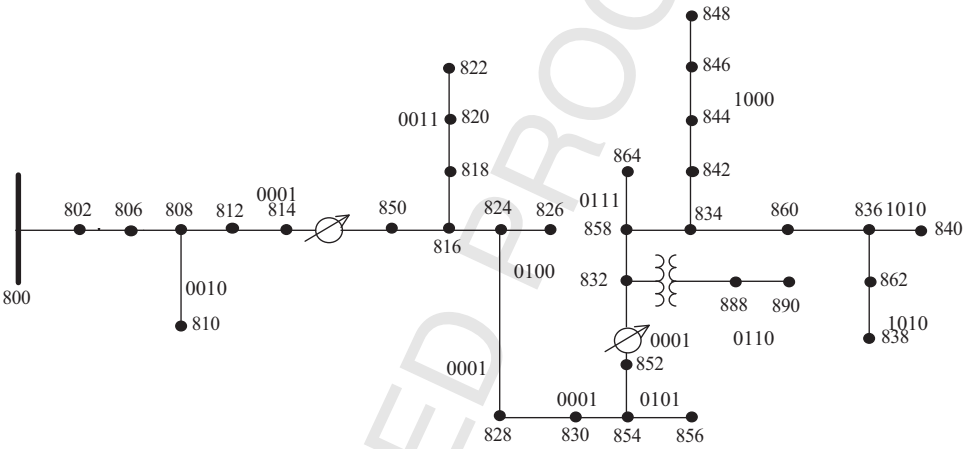

Fig. 5. IEEE 34 node test feeder in DIgSILENT PowerFactory.

used in the generation of the dataset for the training and testing of the FSI and FL ANN models respectively.

3.3. Feature extraction and selection

The three phase and zero sequence line currents from a current transformer located at the substation relaying point of the distribution network given in Fig. 5 is exported to the MATLAB computation platform. The waveforms are sampled at 128 samples per cycle, and decomposed using Daubechies db4 level-6 into their detail and approximation coefficients respectively.

The high pass (g) and low pass (h) filters of the db4 have four coefficients. These are [44,46]:

$$g_1 = 0.1294,\ g_2 = 0.2241,\ g_3 = 0.8365,\ g_4 = 0.4830 \quad (10)$$

$$h_1 = -0.4830,\ h_2 = 0.8365,\ h_3 = -0.2241,\ h_4 = -0.1294 \quad (11)$$

Level-5 DWT detail was selected and the Entropy Per Unit obtained was computed for the 3 phase and zero sequence line currents using Eq. (9). These features were selected because the coefficients obtained from the level-5 DWT decomposition gave the best performance in all the simulations carried out. This is supported by the fact that at level-5, the dominant non-frequency transient that is generated by the faults is observable within the frequency range of 120–240 Hz based on the Nyquist criterion. Also, the wavelet energies and entropy obtained at level-5 were distinctive and consistent. Hence, it was unnecessary to utilize the coefficients from the other scales. Table 3 gives the frequency range for the various decomposition levels based on the sampling frequency used in the decomposition of the fault signal.

The identification of the faulted section and the location of the fault are then predicted based on the type of the fault. Table 4 gives the size of the dataset generated for the training and test-

Table 2
ANN testing simulation parameters.

Parameter	Main feeder (%)	Lateral section (%)
Fault location (%)	15, 25, 45, 50, 60, 85	15, 30, 60, 80, 90
Fault resistance (Ω)	0.5, 2.5, 5	0.5, 2.5, 5
Fault inception angle (°)	0, 30, 45, 60, 90	0, 30, 45, 60, 90
Fault type	Single phase-to-ground (1 Ph.-g), Two phase (2 Ph.), Two phase-to-ground (2 Ph.-g), and Three phase (3 Ph.)	Single phase-to-ground (1 Ph.-g), Two phase (2 Ph.), Two phase-to-ground (2 Ph.-g), and Three phase (3 Ph.)

Table 3
Frequency range for the DWT decomposition level.

Decomposition level	Frequency band (Hz)
D_1	1920–3840
D_2	960–1920
D_3	480–960
D_4	240–480
D_5	120–240
D_6	60–120

Table 4
Summary of the training and test dataset for FSI and FL.

No.	Fault type	Size of training dataset	Size of test dataset
1	Single phase-to-ground	500	100
2	Two phase	400	100
3	Two phase-to-ground	400	100
4	Three phase	150	30

ing of the FSI and FL ANN models using time-domain simulations in DIgSILENT PowerFactory software.

3.4. ANN implementation

In MATLAB, the implementation of the neural networks is performed by means of matrix manipulation of the inputs, outputs, synaptic weights, and bias vectors. The training dataset is presented to the ANN sequentially using batch-mode supervised learning. The weights and the bias of the network are updated based on the error between the network output and the target. The batch-mode iterations continue until the training error obtained is minimized. A search for the number of hidden layer neurons was done to determine the number of hidden layer neurons for the 1 Ph.-g, 2 Ph., 2 Ph.-g, and 3 ph. ANN models. Also, the number of epochs was determined by experimentation. The number of epoch for the training was set between the range of 500 and 3500. An epoch of 500 means the weights are updated with the learning rule continuously until the input dataset has been presented 500 times. The training is repeated for 10 trials, and a Mean Squared Error (MSE) rate of e-03 was used. In the early stopping method, the dataset is randomly divided into three parts: training set (70% of the dataset), validation set (15% of the dataset), and test set (15% of the dataset). The datasets selected for the neural network training are normalized to the range (−1, 1) using Eq. (12) below:

$$l_n = 2 \times \frac{[l - \min(l)]}{[\max(l) - \min(l)]} - 1 \quad (12)$$

where min (l) and max (l) refer to the minimum and maximum values of the input attribute l.

Levenberg–Marquardt (L–M) algorithm was used in updating the weight and bias of the ANN models. The derivation of L–M algorithm starts with the Gauss–Newton (G–N) algorithm. This is given by [46,47]:

$$w^{q+1} = w^q - (J^{qT}J^q)^{-1}J^q e^q \quad (13)$$

where e^q is the error cost function, $q = 1, 2, \ldots, E$ is the iteration index, E is the maximum number of epochs (iterations), w is the weight vector. The Hessian matrix H and the Jacobian matrix J are related by:

$$H = J^T J \quad (14)$$

In order to make the Hessian matrix invertible, an approximation factor known as the identity matrix I is added to it. Such that:

$$H = J^T J + \mu I \quad (15)$$

By combining Eqs. (13) and (15), the update rule is given as:

$$w^{q+1} = w^q - (J^{qT}\mu I)^{-1}J^q e^q \quad (16)$$

where μ is the combination coefficient.

The performance of the trained FSI ANN model is tested using the test dataset. Performance analysis is carried out based on the size of the trained neural network, confusion matrix, classification accuracy, and ability to generalize to untrained datasets. Table 5 presents some of the parameters used in the design of the ANN models for the FSI task.

Table 5
ANN parameters for the FSI and FL tasks.

Parameters	FSI	FL
Input neurons	4	4
Output neurons	4	1
Hidden layer neuron	5:5:25 (1 layer/2 layers)	5:5:25 (1 layer)
Training algorithm	Scaled conjugate gradient (SCG)	Levenberg–Marquardt (LM)
Activation function (hidden layer)	*tansig*	*tansig*
Activation function (output layer)	*tansig*	*purelin*
Weight update method	Batch-mode	Batch-mode

Table 6
Binary notation representing the various line sections.

No.	Section	Classification class			
1	Main feeder	0	0	0	1
2	Lateral 808–810	0	0	1	0
3	Lateral 816–822	0	0	1	1
4	Lateral 824–826	0	1	0	0
5	Lateral 854–856	0	1	0	1
6	Lateral 832–890	0	1	1	0
7	Lateral 858–864	0	1	1	1
8	Lateral 834–848	1	0	0	0
9	Lateral 836–838	1	0	0	1
10	Lateral 836–840	1	0	1	0

For the FSI task, the ANN models use four inputs obtained from the Entropy Per Unit (EPU) of the three phase and zero sequence line current DWT coefficients. The output of the FSI ANN models is the fault section in the distribution network denoted by the binary notations in Fig. 5. The binary notation used is given in Table 6. Similarly, for the FL task, the ANNs use four inputs obtained from the Entropy Per Unit (EPU) of the three phase and zero sequence line current DWT coefficients. The output of the FL ANN models is the location of the fault in kilometres.

The absolute relative error (RE_{abs}) is calculated using Eq. (17), and it is a function of the actual fault location and the total length of the line. Unlike a transmission network, it would be erroneous to use the total length of the distribution network or the total length of the main feeder in Eq. (17). In this regard, the length of the lateral where the fault occurred is taken as the length of the line in computing the absolute relative error. The length for the various line segments is calculated from the beginning of the feeder (node 800) to the end of the lateral. Table 7 gives the total length of the various segments in the test feeder.

$$RE_{abs} = \frac{|\text{Actual Location} - \text{Estimated Location}|}{\text{Length of Line}} \times 100\% \quad (17)$$

Table 7
Feeder/lateral lengths.

No.	Line section	Feeder/lateral length (km)
1	Main feeder	57.415
2	Lateral 808–810	12.907
3	Lateral 816–822	51.112
4	Lateral 824–826	35.762
5	Lateral 854–856	48.594
6	Lateral 832–890	55.930
7	Lateral 858–864	54.699
8	Lateral 834–848	57.750
9	Lateral 836–838	58.982
10	Lateral 836–840	57.677

Please cite this article in press as: A.C. Adewole, et al., Distribution network fault section identification and fault location using wavelet entropy and neural networks, Appl. Soft Comput. J. (2016), http://dx.doi.org/10.1016/j.asoc.2016.05.013

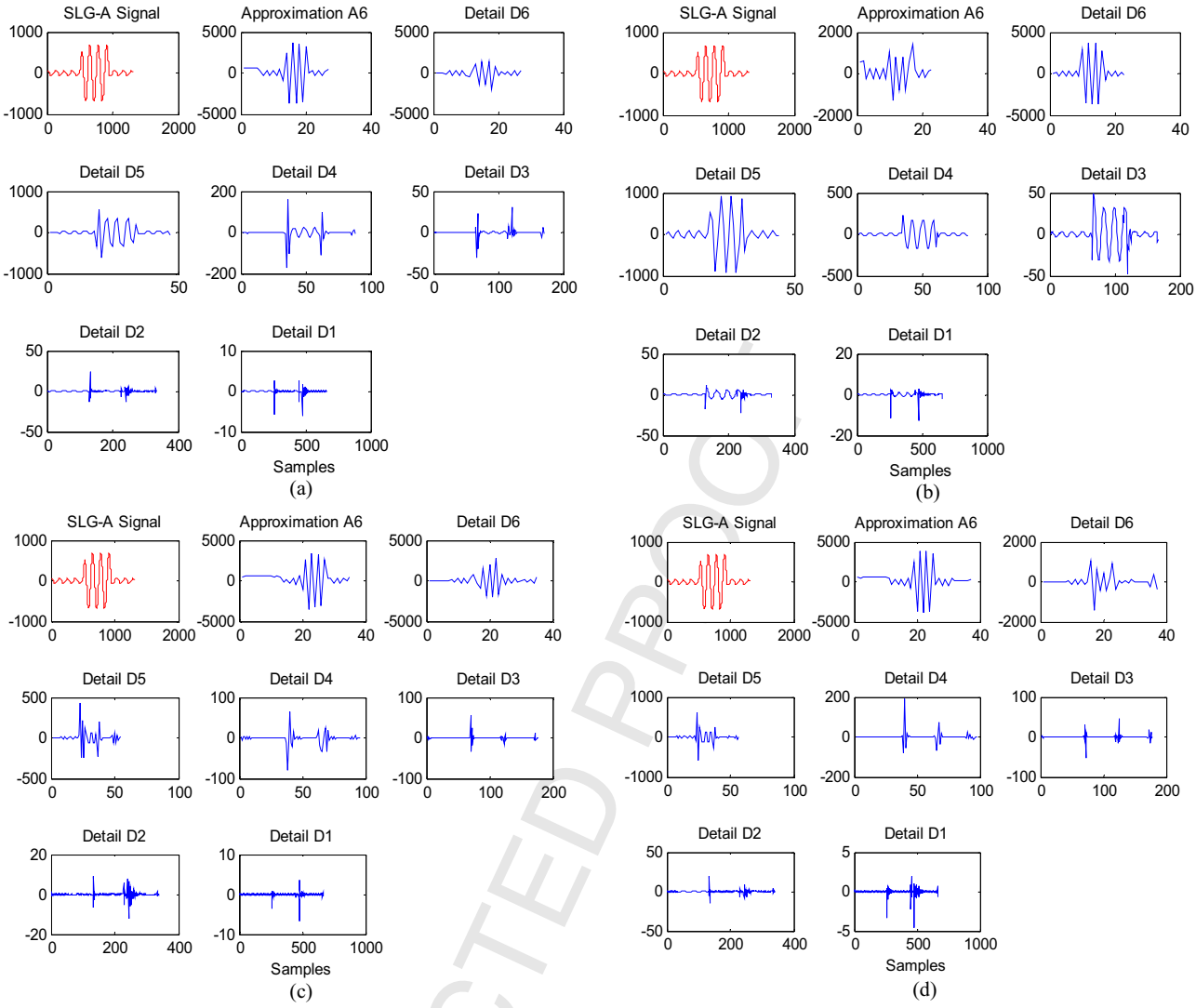

Fig. 6. Wavelet decomposition of A–g fault at line 806–808 using (a) db4 mother wavelet; (b) db2 mother wavelet; (c) db8 mother wavelet; and (d) Coiflet-3 mother wavelet.

4. Results and discussion

Extensive simulation studies have been carried out to test and validate the proposed hybrid method. However, only some of the results of the simulation studies carried out are reported due to lack of space. Fig. 6 shows the DWT decomposition using various mother wavelets for a 1 Ph.g (phase A-to-ground) fault at the line segment 806–808, where SLG-A is the single line-to-ground fault for phase A of the distribution network. Line 806–808 is at 10% of the length of the main feeder. Spikes are noticeable at the instant of the fault inception.

Table 8 shows the wavelet energy spectrum entropy computed for the above-mentioned fault using Eq. (9). From Fig. 6, it can be seen that the detail signal at level-5 gave the best reflection of the original transient signal before and after the inception of the fault. Also, exploratory investigations carried out for various levels of decomposition like in Table 8 showed that the results obtained at level-5 of the DWT decomposition demonstrated consistency for the various scenarios investigated. This is indicated by the low relative wavelet energy spectrum entropy computed for the faulted phase.

Table 8
Entropy indices for A–g fault at line 806-808.

Scales	WEE_A	WEE_B	WEE_C	WEE_{I0}
Level-1	2.5374	3.7492	3.8123	3.5551
Level-2	2.0987	3.1031	3.1321	2.7209
Level-3	2.6984	2.5938	3.0079	2.7935
Level-4	2.7467	4.412	4.4197	2.8112
Level-5	3.7374	5.1914	4.5281	3.5526
Level-6	3.1647	4.5726	3.9347	2.7917

For the FSI task, the ANN training using the Scaled Conjugate Gradient (SCG) training algorithm was faster and gave better performance than the Levenberg–Marquardt (L–M) training algorithm. The confusion matrices obtained during the training of the 1 Ph. and 3 Ph. ANN models are given in Fig. 7. The green squares give the correct response per prediction class for the ANN models, while the red squares indicate the incorrect responses. The accuracy per output class is given by the grey squares, and the blue squares present the overall accuracy of the ANN model. The processor and CPU usages obtained during the training of the FSI ANN model for 1 Ph.g is shown in Fig. 8.

Tables 9 and 10 present a comparative analysis of the performance of the ANN models obtained using the EPU and WEE inputs for the training of 1 Ph.g and 3 Ph. FSI ANN models respectively. From the tables, it can be seen that the ANN model trained using EPU inputs generally gave better prediction accuracy, had faster computation time, and used less processor and memory compared

Please cite this article in press as: A.C. Adewole, et al., Distribution network fault section identification and fault location using wavelet entropy and neural networks, Appl. Soft Comput. J. (2016), http://dx.doi.org/10.1016/j.asoc.2016.05.013

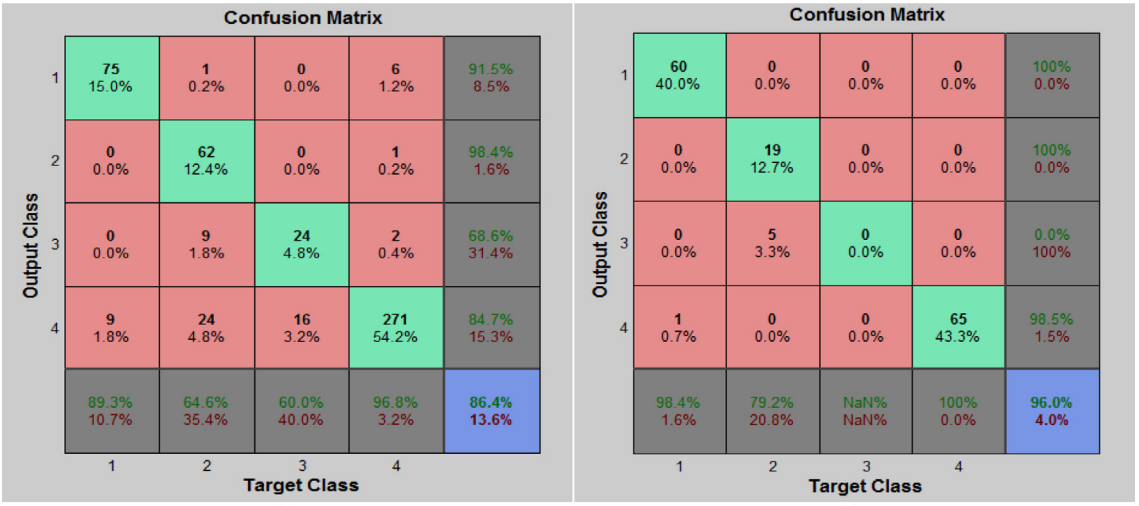

(a) (b)

Fig. 7. Confusion matrices for (a) 1 Ph.g FSI ANN model (4-10-10-4); and (b) 3 Ph. FSI ANN (4-20-20-4) model.

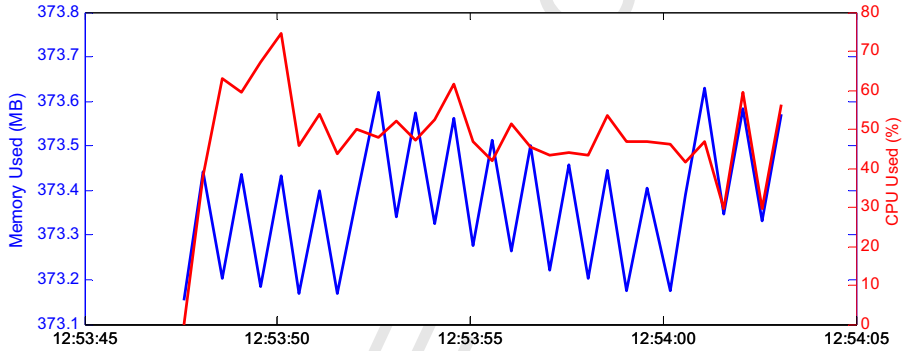

Fig. 8. Processor (CPU) usage and memory usage plots for 1 Ph.g FSI ANN model (4-20-20-4).

Table 9
Comparative analysis of ANN models based on EPU and WEE inputs for FSI (1 Ph.).

ANN structure	EPU prediction accuracy (%)	WEE prediction accuracy (%)	EPU mean computation time (s)	WEE mean computation time (s)	EPU mean memory usage (MB)	WEE mean memory usage (MB)	EPU mean CPU usage (%)	WEE mean CPU usage (%)
4-5-4	70.8	70.6	10.53	10.92	192.65	31929	43.33	44.78
4-10-4	73.4	73.4	11.07	32.32	320.07	261.49	49.44	40.13
4-20-4	78.8	83.8	12.07	15.17	324.88	308.93	51.61	41.53
4-5-5-4	81.8	78.8	11.02	13.27	236.45	319.80	59.28	44.01
4-10-10-4	86.4	83.4	11.51	13.19	222.83	320.91	50.93	48.54
4-20-20-4	87.2	85.2	14.12	15.98	360.28	306.92	47.20	49.81

Table 10
Comparative analysis of ANN models based on EPU and WEE inputs for FSI (3 Ph.).

ANN structure	EPU prediction accuracy (%)	WEE prediction accuracy (%)	EPU mean computation time (s)	WEE mean computation time (s)	EPU mean memory usage (MB)	WEE mean memory usage (MB)	EPU mean CPU usage (%)	WEE mean CPU usage (%)
4-5-4	85.3	80.7	9.99	9.93	332.09	327.19	46.78	45.82
4-10-4	94.0	87.3	10.19	9.61	333.72	328.42	39.80	53.14
4-20-4	90.0	86.7	12.30	11.68	337.26	329.52	72.37	60.96
4-5-5-4	88.0	86.7	10.89	11.72	318.34	317.48	40.55	46.65
4-10-10-4	91.3	86.7	11.44	11.14	318.47	314.71	40.35	47.46
4-20-20-4	96.0	92.0	13.20	12.13	308.50	325.71	53.57	48.28

Table 11
Summary of results for FSI ANN models.

Fault type	Final ANN structure	MSE	Confusion matrix (%)	Test accuracy (%)
Single phase-to-ground	4-10-10-4	0.01967	86.4	89.0
Two phase	4-20-4	0.01188	92.4	91.0
Two phase-to-ground	4-10-4	0.01770	96.4	89.0
Three phase	4-10-4	0.02443	94.0	93.3

Please cite this article in press as: A.C. Adewole, et al., Distribution network fault section identification and fault location using wavelet entropy and neural networks, Appl. Soft Comput. J. (2016), http://dx.doi.org/10.1016/j.asoc.2016.05.013

Table 12
Comparative analysis of ANN models based on EPU and WEE inputs for FL (1 Ph.g).

ANN structure	EPU regression coefficient	WEE regression coefficient	EPU mean computation time (s)	WEE mean computation time (s)	EPU mean memory usage (MB)	WEE mean memory usage (MB)	EPU mean CPU usage (%)	WEE mean CPU usage (%)
4-5-1	0.92214	0.93679	3.55	4.13	316.04	316.12	39.26	34.28
4-10-1	0.93506	0.9792	4.95	9.80	310.88	338.32	49.21	31.80
4-20-1	0.96860	0.97321	6.64	4.05	320.41	342.30	47.70	33.84

Table 13
Comparative analysis of ANN models based on EPU and WEE inputs for FL (3 Ph.).

ANN structure	EPU regression coefficient	WEE regression coefficient	EPU mean computation time (s)	WEE mean computation time (s)	EPU mean memory usage (MB)	WEE mean memory usage (MB)	EPU mean CPU usage (%)	WEE mean CPU usage (%)
4-5-1	0.92918	0.96379	3.57	3.66	307.68	312.53	38.82	30.07
4-10-1	0.99995	0.98022	4.21	2.94	310.28	321.87	35.47	32.58
4-20-1	0.99993	0.99066	3.23	3.13	315.25	331.65	41.13	32.09

Table 14
Summary of results for FL ANN models.

Fault type	Final ANN structure	Regression coefficient	Max/min fault location relative error (%)
Single phase-to-ground	4-20-1	0.9686	1.07/0.13
Two phase	4-15-15-1	0.9976	1.20/0.70
Two phase-to-ground	4-10-10-1	0.9998	0.55/0.10
Three phase	4-10-1	0.9999	0.28/0.01

Table 15
Performance analysis of the FSI and FL algorithms.

Test parameters					Test results		
Fault type	Fault resistance (Ω)	Fault inception angle (°)	Fault section	Fault location (km)	Fault section	Fault location (km)	Relative error (%)
B–g	2.5	30	0100	34.9667	0100	34.4154	1.54
B–g	2.5	30	0101	45.0388	0101	45.7185	1.40
B–g	2.5	60	0101	42.0388	0101	41.2929	1.53
A–g	2.5	30	0111	54.4525	0111	53.7322	1.32
A–g	2.5	60	0111	53.4525	0111	52.5596	1.63
BCg	0.5	45	1000	56.2737	1000	56.6047	0.57
C–g	2.5	30	1001	55.9251	1001	54.8790	1.77
C–g	5.0	30	1001	57.9251	1001	58.7004	1.31
C–g	2.5	60	1001	57.4920	1001	57.6935	0.34
C–g	5.0	60	1001	57.4920	1001	56.8563	1.08
AB	0.5	0.0	1000	56.2737	1000	57.2357	1.67
AB	0.5	30	0001	25.8673	0001	25.8466	0.04
ABg	0.5	30	1001	57.4920	1001	57.1873	0.52
ABg	0.5	30	1010	57.4807	1010	57.1878	0.51
BCg	0.5	30	1010	57.4807	1010	58.3439	1.50
CAg	0.5	30	1010	57.4807	1010	57.7271	0.43
ABC	0.5	60	1010	57.4807	1010	57.7681	0.50
A–g	**100**	**30**	**0110**	**52.3215**	**1001**	**51.4287**	**1.60**

to the ANN models trained using WEE inputs. The final ANN models chosen for the FSI task are given in Table 11. The format used for the final structures of the ANN models in Table 11 is *Input-Hidden layer-Output*. For example, for single phase-to-ground faults, the FSI ANN model consists of 4 neurons in the input layer, 2 hidden layers with 10 neurons each, and 4 neurons in the output layer respectively. The final ANN models were selected based on the prediction accuracy obtained, computation time, and processor/memory usages. It is important that the chosen ANN models have lower footprints in terms of computation time and processor/memory usages. This is necessary for real-time implementation, field deployment, and ANN retraining.

For the FL task, the ANN models trained using WEE inputs gave more accurate results compared to ANN models trained using EPU inputs as shown in Tables 12 and 13 for the 1 Ph.g and 3 Ph. ANN models respectively. However, the computation time and mean processor usage were greater for the WEE-based ANN models compared to the EPU-based ANN models. The final ANN models chosen for the FL task are given in Table 14.

Table 15 presents the performance test of the method using untrained dataset for fault locations, fault inception angles, and fault resistances different from those used in training the ANN models. Very promising results were obtained. The FSI ANN model for 1 Ph.-g faults misclassified adjacent faulted sections (lateral 836–838 and lateral 836–840) at high fault resistance as shown by the text in bold in Table 15. However, the predicted fault location with 1.60 relative percentage error was still within acceptable margin based on the specifications of commercially available fault locators implemented in substation Intelligent Electronic Devices (IEDs)/protection relays, which are usually specified with a max-

Table 16
Performance comparison with some existing methods.

Method	Maximum error recorded (%)	
	A–g	ABC-g
Proposed method	1.60	0.50
Impedance-based [13]	1.53	0.96
Impedance-based [14]	6.01	0.50
Impedance-based [18]	1.77	2.66
Impedance-based [19]	1.85	2.76
ANN & impedance-based [23]	4.57	1.48
ANN-based [32]	Not considered	6.30

imum relative percentage error of 5.0 as given in Refs. [48,49]. Table 16 gives a comparative analysis of the proposed method with some existing methods in the literature.

5. Conclusion

This paper has developed a hybrid 2-stage method for distribution network fault section identification (FSI) and fault location (FL) based on the coefficients from level-5 detail coefficients obtained from DWT decomposition using db4 mother wavelet. Wavelet Energy Spectrum Entropy (WEE) and Entropy Per Unit (EPU) indices are computed from the DWT detail coefficients. These indices are used in training artificial neural network models for the FSI and FL tasks respectively. Comparison of ANN models trained using the EPU and WEE indices is carried out in terms of the prediction accuracy, computation time, processor usage, and memory usage. In order to validate the proposed hybrid method, it is applied to the IEEE 34-node benchmark test feeder. The proposed method can easily be implemented practically using actual data obtained from Digital Fault Recorders (DFR) or Intelligent Electronic Devices (IEDs). Although, data obtained from DFRs/IEDs are usually noisy, the noise would be filtered out as a result of the DWT decomposition. The ANN models trained using EPU indices were shown to require less computer memory, less processor usage, and gave faster computation speed.

The robustness of the proposed hybrid method to various fault resistance, fault types, fault inception angle, and fault location was demonstrated. Accurate results irrespective of fault locations, fault resistances, fault inception angles, and fault types were obtained for the FSI and FL tasks respectively. The proposed 2-stage hybrid method is suitable for practical deployment in distribution network control centres because of its simplicity and accuracy, and can be used to aid engineers and control centre dispatchers in fault diagnosis. It should be noted that since the proposed hybrid method uses only line current signals available from current transformers already existing in substations, there is no added cost involved in the roll-out (implementation) of the proposed hybrid method.

Possible future extension of the proposed hybrid method could be in the use of synchrophasor measurements from Phasor Measurement Units (PMUs). Also, machine learning classifiers and predictors based on decision trees/ensembles of decision trees can be applied to identify the faulted section and the location of the fault in the power system distribution network.

Acknowledgements

Q6 This research work is funded by the South African National Research Foundation (NRF) THRIP Grant TP2011061100004 “CSAEMS development and growth”. The authors are grateful for the financial support.

References

[1] M.M. Saha, J. Izykowski, E. Rosolowski, Fault Location on Power Networks, Springer-Verlag Limited, 2010, pp. 8.
[2] A.C. Adewole, R. Tzoneva, A review of methodologies for fault detection and location in distribution power networks, Int. Rev. Model. Simul. 4 (2011) 3214–3231.
[3] T. Takagi, Y. Yamakoshi, Y. Yamaura, R. Kondow, T. Matsushima, Development of a new type fault locator using the one terminal voltage and current data, IEEE Trans. Power Appar. Syst. 101 (1982) 2892–2898.
[4] L. Eriksson, M.M. Saha, G.D. Rockefeller, An accurate fault locator with compensation for apparent reactance in the fault resistance resulting from remote-end infeed, IEEE Trans. Power Appar. Syst. 104 (1985) 424–436.
[5] A.T. Johns, S. Jamali, Accurate fault location technique for power transmission Q7 lines, IEEE Proc. 137 (1990) 395–402.
[6] D. Novosel, D.G. Hart, E. Udren, J. Garitty, Unsynchronized two terminal fault location estimation, IEEE Trans. Power Deliv. 11 (1986) 130–138.
[7] Z. Chen, J.C. Maun, Artificial neural network approach to single-ended fault locator for transmission lines, IEEE Trans. Power Syst. 15 (2000) 370–375.
[8] Z.E. Aygen, S. Seker, M. Bagnyanik, F.G. Bagnyanik, E. Ayaz, Fault section estimation in electrical power systems using artificial neural network approach, IEEE Transmission and Distribution Conference 2 (1999) 466–469.
[9] P.S. Bhowmik, P. Purkait, K. Bhattacharya, A novel wavelet transform aided neural network based transmission line fault analysis method, Electric Power Energy Syst. 31 (2009) 213–219.
[10] S. Hongchun, S. Xiangfei, A new method for locating faults on transmission lines based on rough set and FNN, International Conference on Power System Technology (2002) 2584–2588.
[11] J. Sadeh, H. Afradi, A new and accurate fault location algorithm for combined transmission lines using adaptive network-based fuzzy inference system, Electr. Power Syst. Res. 79 (2009) 1538–1545.
[12] A.A. Girgis, C.M. Fallon, D.L. Lubkerman, A fault location technique for rural distribution feeder, IEEE Trans. Ind. Appl. 29 (1993) 1170–1175.
[13] G.D. Ferreira, D. da S. Gazzana, A.S. Bretas, A.H. Ferreira, A.L. Bettiol, A. Carniato, Impedance-Based Fault Location for Overhead and Underground Distribution Systems, North American Power Symposium (2012) 1–6.
[14] J.J. Mora-Florez, R.A. Herrera-Orozco, A.F. Bedoya-Cadena, Fault location considering load uncertainty and distributed generation in power distribution systems, IET, Generation Transmission, Distribution 9 (2015) 287–295.
[15] M.M. Saha, E. Rosolowski, J. Izykowski, ATP-EMTP investigation for fault location in medium voltage networks, International Conference on Power Systems Transients (IPST'05) 05–220 (2005) 1–6.
[16] R.A.F. Pereira, M. Kezunovic, J.R.S. Mantovani, Fault location algorithm for primary distribution feeders based on voltage sags, Int. J. Innov. Energy Syst. Power 4 (2009) 1–8.
[17] G. Morales-España, J. Mora-Flórez, H. Vargas-Torres, Elimination of multiple estimation for fault location in radial power systems by using fundamental single-end measurements, IEEE Trans. Power Deliv. 24 (2009) 1382–1389.
[18] R.H. Salim, M. Resener, A.D. Filomena, K.R. Caino De Oliveira, A.S. Bretas, Extended fault-location formulation for power distribution systems, IEEE Trans. Power Deliv. 24 (2009) 508–516.
[19] A.D. Filomena, M. Resener, R.H. Salim, A.S. Bretas, Fault location for underground distribution feeders: an extended impedance-based formulation with capacitive current compensation, Electr. Power Energy Syst. 31 (2009) 489–496.
[20] F.H. Magnago, A. Abur, A new fault location technique for radial distribution systems based on high frequency signals, IEEE Power Engineering Society Summer Meeting 1 (2009) 426–431.
[21] D.W.P. Thomas, R.J.O. Carvalho, E.T. Pereira, Fault location in distribution systems based on traveling wave, Proceedings of IEEE Bologna Power Technology Conference (2003) 468–472.
[22] A. Borghetti, M. Bosetti, M. Di Silvestro, C.A. Nucci, M. Paolone, Continuous-wavelet transform for fault location in distribution power networks: definition of mother wavelets inferred from fault originated transients, International Conference on Power Systems Transients (IPST'07) (2007) 1–9.
[23] R.H. Salim, K.R. Caino de Oliveira, A.D. Filomena, M. Resener, A.S. Bretas, Hybrid fault diagnosis scheme implementation for power distribution systems automation, IEEE Trans. Power Deliv. 23 (2008) 1846–1856.
[24] M.T. Yang, J.L. Guan, J.C. Gu, High impedance faults detection technique based on wavelet transform, World Acad. Sci. Eng. Technol. (28) (2016) 308–312.
[25] H. Hizam, P.A. Crossley, Estimation of fault location on a radial distribution network using fault generated travelling waves signal, J. Appl. Sci. 7 (2007) 3736–3742.
[26] U.D. Dwivedi, S.N. Singh, S.C. Srivastava, A wavelet based approach for classification and location of faults in distribution systems, Annual IEEE India Conference, INDICO 2 (2008) 488–493.
[27] W. Zhao, Y.H. Song, Y. Min, Wavelet analysis based scheme for fault detection and classification in underground power cable systems, Proc. Electr. Power Syst. Res. 53 (2000) 23–30.
[28] K.L. Butler-Purry, J. Cardoso, Characterization of underground cable incipient behavior using time-frequency multi-resolution analysis and artificial neural networks, Proceedings of IEEE Power and Energy Society General Meeting—Conversion and Delivery of Electrical Energy in the 21st Century (2009) 1–11.

Please cite this article in press as: A.C. Adewole, et al., Distribution network fault section identification and fault location using wavelet entropy and neural networks, Appl. Soft Comput. J. (2016), http://dx.doi.org/10.1016/j.asoc.2016.05.013

[29] C.Y. Teo, Automation of knowledge acquisition and representation of fault diagnosis in power distribution networks, Electr. Power Syst. Res. 27 (1993) 183–189.
[30] E.A. Mohamed, N.D. Rao, Artificial neural network fault diagnostic system for electric power distribution feeders, Electr. Power Syst. Res. 35 (1995) 1–10.
[31] D.T.W. Chan, C.Z. Lu, Distribution system fault identification by mapping of characteristic vectors, Electr. Power Syst. Res. 57 (2001) 15–23.
[32] M. Al-Shaher, M.M. Sabra, A.S. Saleh, Fault location in multi-ring distribution network using artificial neural network, Electr. Power Syst. Res. 64 (2003) 87–92.
[33] L.S. Martins, V.F. Pires, C.M. Alegria, A new accurate fault location method using αβ space vector algorithm, Proceeding of 14th PSCC 3 (2002) 1–6.
[34] J. Mora-Flórez, J. Cormane-Angarita, G. Ordó˜nez-Plata, K-means algorithm and mixture distributions for locating faults in power systems, Electr. Power Syst. Res. 79 (2009) 714–721.
[35] D. Thukaram, H.P. Khincha, H. Vijaynarasimha, Artificial neural network and support vector machine approach for locating faults in radial distribution systems, IEEE Trans. Power Deliv. 20 (2005) 710–721.
[36] F. Chunju, K.K. Li, W.L. Chan, Y. Weiyong, Z. Zhaoning, Application of wavelet fuzzy neural network in locating single line to ground fault (SLG) in distribution lines, Electr. Power Energy Syst. 29 (2007) 497–503.
[37] A.C. Adewole, Investigations of Methodologies for Fault Detection and Diagnosis in Electric Power System Protection, Master's Thesis, Department of Electrical Engineering, Cape Peninsula University of Technology, South Africa, 2012.
[38] A.C. Adewole, R. Tzoneva, Distribution network fault detection and diagnosis using waveform energy spectrum entropy and neural networks, Int. Rev. Electr. Eng. 9 (2014) 165–173.
[39] S.R. Samantaray, B.K. Panigrahi, P.K. Dash, High impedance fault detection in power distribution networks using time-frequency transform and probabilistic neural network, IET, Generation, Transmission and Distribution 2 (2008) 261–270.
[40] H. Zhengyou, F. Ling, L. Sheng, B. Zhiqian, Fault detection and classification in EHV transmission line based on wavelet singular entropy, IEEE Trans. Power Deliv. 25 (2010) 2156–2163.
[41] S. Ekici, S. Yildirim, M. Poyraz, Energy and entropy-based feature extraction for locating fault on transmission lines by using neural network and wavelet packet decomposition, Expert Syst. Appl. 34 (2008) 2937–2944.
[42] B.K. Panigrahi, V.R. Pandi, Optimal feature selection for classification of power quality disturbances using wavelet packet-based fuzzy k-nearest neighbor algorithm, IET, Generation, Transmission, Distribution 3 (2009) 296–306.
[43] A. Borghetti, M. Bosetti, M. Di Silvestro, C.A. Nucci, M. Paolone, Continuous-Wavelet Transform for Fault Location in Distribution Power Networks: Definition of Mother Wavelets Inferred From Fault Originated Transients (IPST'07) (2007) 1–9.
[44] I. Daubechies, Ten Lectures on Wavelets, SIAM, 1992. Q8
[45] http://www.ewh.ieee.org/soc/pes/dsacom/testfeeders.html.
[46] H. Demuth, M. Beale, M. Hagan, Neural Network Toolbox for Use with MATLAB, Users Guide Version 4, 2004.
[47] C.M. Bishop, Neural Networks for Pattern Recognition, Oxford University Press, 1996.
[48] A. Sauhats, A. Jonins, M. Danilova, Statistical adaptive algorithms for fault location on power transmission lines based on method of Monte-Carlo, in: Proc. 7th International Conference on Probabilistic Methods Applied to Power Systems, September 22–26, 2002, Naples, Italy, 2002, pp. 485–490.
[49] General Electric F650 Digital Bay Controller Instructions Manual (2014).

Please cite this article in press as: A.C. Adewole, et al., Distribution network fault section identification and fault location using wavelet entropy and neural networks, Appl. Soft Comput. J. (2016), http://dx.doi.org/10.1016/j.asoc.2016.05.013